Paper
Int'l J. of Aeronautical & Space Sci. 16(1), 102–109 (2015)
DOI: http://dx.doi.org/10.5139/IJASS.2015.16.1.102

IJASS
International Journal of Aeronautical and Space Sciences

Path Tracking Controller Design and Simulation for Korean Lunar Lander Demonstrator

Sungwook Yang*, Jongjun Son and Sangchul Lee*****

Korea Aerospace University, Goyang 412-791, Korea

Abstract

In Korea, Lunar exploration program has been prepared with the aim of launching in the 2020's. As a part of it, a lunar lander demonstrator was developed, which was the model for verifying the system such as structure, propulsion, and control system, before launching into the deep space. This paper deals with the path tracking performance of the lunar lander demonstrator with respect to the thruster controller based on Pulse Width Pulse Frequency Modulator (PWPFM) and Pulse Width Modulator (PWM). First, we derived equations of motion, considering the allocation of the thrusters, and designed the path tracking controller based on Euler angle. The signal generated from the path tracking controller is continuous, so PWPFM and PWM modulator are adopted for generating ON/OFF signal. Finally, MATLAB simulation is performed for evaluating the path tracking ability. We compared the path tracking performances of PWPFM and PWM based thrust controller, using performance measures such as the total impulse and the position error with respect to the desired path.

Key words: Lunar Lander Demonstrator, Thrust Controller, PWPFM, PWM, Path Tracking Controller

1. Introduction

In Korea, Lunar exploration program has been prepared with the aim of launching in the 2020's. As a part of it, a lunar lander demonstrator has been developed, which is the model for verifying the system such as structure, propulsion, and control system, before launching into the deep space. After verifying the system, the demonstrator will be evaluated by flight test including ascent, horizontal movement, descent, and touchdown phase. The flight test scenario was defined by considering the final descent phase and touchdown phase of actual lunar landing mission [1]. The performance index of the control system would be final velocity, path tracking ability, etc. Therefore, precise model and controller are necessary [2].

Typical thruster control systems are thrust vector control (TVC) systems and reaction control system(RCS), which are commonly used for many launch vehicles worldwide. Masten space system developed a demonstrator to which the TVC was applied, and NASA is developing the Warm Gas Test Article(WGTA) by adopting the RCS. [3-4]

The signal generated from the controller is continuous, so modulation is necessary for generating ON /OFF signal. In general, bang-bang control, Schmitt trigger control, pulse width modulator (PWM), and pulse width pulse frequency modulator (PWPFM) are used for ON /OFF control. The PWM can be used in a quasilinear mode, by modulating the width of the reaction pulse proportionally to the level of the commanded torque input to the controller. A related technique is based on the well-known Schmidt trigger, which implements a PWPFM where the distance between the pulses is also modulated [5].

In this paper, the dynamic equations for the motion of the lunar lander demonstrator are derived, considering the allocation of thrusters. Next, we designed the path tracking controller based on Euler angle. In order to generate ON/OFF signal, PWPFM and PWM modulators were adopted. Finally, computer simulations were performed for evaluating the path tracking ability and comparing the path tracking performance between PWPFM and PWM based thruster controller. For the

* Ph. D Student, Corresponding Author: sungwooky@kau.ac.kr
** MD Student
*** Professor

Received: February 2, 2015 Revised: March 19, 2015 Accepted: March 23, 2015

http://ijass.org pISSN: 2093-274x eISSN: 2093-2480

performance measure, the total impulse [6] and the position error, with respect to the desired path, were used.

2. Dynamic Modelling

X, Y, Z is an inertial frame, and x_b, y_b, z_b is a frame which is attached at the center of mass as shown in Fig. 1.

2.1 Consideration of Thrusters Allocation

The demonstrator has main thrusters, which can be used for altitude control, and reaction thrusters, which can be used for attitude control. The arrangement of the thrusters is illustrated in Fig. 2; the force generated from i th thruster is

$$\mathbf{F}_i = \begin{bmatrix} F_{x_i} \\ F_{y_i} \\ F_{z_i} \end{bmatrix} = -\begin{bmatrix} -\cos(\alpha_i) \\ \sin(\alpha_i)\cos(\beta_i) \\ \sin(\alpha_i)\sin(\beta_i) \end{bmatrix} F_i \tag{1}$$

The torque generated from total thrusters is as follows.

$$\mathbf{T} = \sum_{i=1}^{N} \mathbf{r}_i \times \mathbf{F}_i \tag{2}$$

2.2 Equations of Motion

Using Newton-Euler equations, we can represent the dynamics of the demonstrator as follows.

$$I_b \cdot \dot{\boldsymbol{\omega}} + \boldsymbol{\omega}^{\times} I_b \boldsymbol{\omega} = \mathbf{T}_{m.t} + \mathbf{T}_{r.t} = \mathbf{T}_{total} \tag{3}$$

$$m\dot{\mathbf{V}} + \boldsymbol{\omega} \times (m\mathbf{V}) = \mathbf{F}_{m.t} + \mathbf{F}_{r.t} + \mathbf{F}_g = \mathbf{F}_{total} \tag{4}$$

$$\dot{\boldsymbol{\xi}} = \boldsymbol{\omega} \tag{5}$$

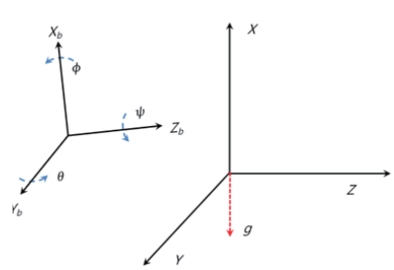

Fig. 1. Inertial Frame and Body Frame

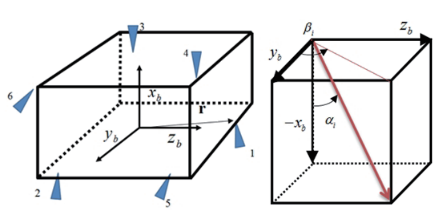

Fig. 2. Allocation and Direction of Thrusters

where $\boldsymbol{\omega}_b=[\omega_x, \omega_y, \omega_z)]^T$ denotes the angular velocity vector with respect to the body frame, $\times$ denotes the vector cross product, I_b is the inertia matrix of demonstrator, $\boldsymbol{T}_{m.t}=[\tau_{m.t_x}, \tau_{m.t_y}, \tau_{m.t_z}]^T$ is torque generated by main thrusters, $\boldsymbol{T}_{r.t}=[\tau_{r.t_x}, \tau_{r.t_y}, \tau_{r.t_z}]^T$ is torque generated by reaction thrusters, m is total mass of the demonstrator, $\boldsymbol{V}_b=[\dot{x}_b \quad \dot{y}_b \quad \dot{z}_b]^T$ is linear velocity with respect to body frame, $\boldsymbol{F}_{m.t}=[F_{m.t}, 0, 0]^T$ is the total force generated by main thrusters, $\boldsymbol{F}_{r.t}=[\tau_{r.t_x}, \tau_{r.t_y}, \tau_{r.t_z}]^T$ is the total force generated by reaction thrusters, and $\boldsymbol{F}_g=[F_{g_x}, F_{g_y}, F_{g_z}]^T$ is the gravity force with respect to body frame, $\boldsymbol{\xi} = [\phi \quad \theta \quad \psi]^T$ is Euler angle.

2.3 Thruster Modeling

Simple thruster models assume a thrust profile as a square pulse; however, the response can be different. So, suitable approximations may be used to increase robustness and form a premise for making more precise maneuvers. In this paper, the general dynamic model is used to be realistic, as follows [6].

$$T\dot{u} + u = v \tag{6}$$

where T is positive constant, u is an actual control input, and v is desired actuator input.

3. Design Controller

The demonstrator is assumed as an under actuated platform, so it can track the path by changing the attitude.

3.1 Euler angle based controller

The demonstrator model given in the previous section is a complicated, non-linear system. Equations (3) and (4) can be simplified under the following assumption. [7]

① $F_{total} \gg \boldsymbol{\omega} \times (m\boldsymbol{V})$
② $T_{total} \gg \boldsymbol{\omega} \times (I_b \boldsymbol{\omega})$
③ $\boldsymbol{F}_{m.t} + \boldsymbol{F}_{r.t} \cong \boldsymbol{F}_{m.t}$
④ The angular displacement of θ and ψ are small.

This leads to the following dynamical equations based on Euler angle:

$$m\ddot{x} = (\cos\theta\cos\psi)F_{m.t} - mg \tag{7}$$

$$m\ddot{y} = (\sin\phi\sin\theta\cos\psi + \cos\phi\sin\psi)F_{m.t} \tag{8}$$

$$m\ddot{z} = (\sin\phi\sin\psi - \cos\phi\sin\theta\cos\psi)F_{m.t} \tag{9}$$

where ϕ, θ, ψ are the 1-2-3 set of Euler angles. $\ddot{x}$, $\ddot{y}$, $\ddot{z}$ are the acceleration with respect to the inertial frame.

The altitude can be controlled by simple PD controllers, using Eq. (6).

$$u_1 = m\left(\frac{g + K_{p1}(x_d - x) + K_{d1}(\dot{x}_d - \dot{x})}{cos\theta cos\psi}\right) \tag{10}$$

ϕ can be controlled by simple PD controllers, using as follows;

$$u_2 = K_{p2}(\phi_d - \phi) + K_{d2}(\dot{\phi}_d - \dot{\phi}) \tag{11}$$

y axis is related to the ψ by Eq. (4). We designed a proportional derivative (PD) controller to control the ψ in order to control y motion. From Eq. (7), setting ϕ=θ=0 and $F_{m.t}$=m gives

$$\psi_d = sin^{-1}\left[K_p(y_d - y) + K_d(\dot{y}_d - \dot{y})\right] \tag{12}$$

From Eq. (11), the command torque u_3 is as follows;

$$u_3 = K_{p3}(\psi_d - \psi) + K_{d3}(\dot{\psi}_d - \dot{\psi}) \tag{13}$$

z axis is related to the θ by Eq. (8). We designed a proportional derivative(PD) controller to control the θ in order to control z motion. From Eq. (8), setting ϕ=ψ=0 and $F_{m.t}$=m gives

$$\theta_d = sin^{-1}\left[-K_p(z_d - z) - K_d(\dot{z}_d - \dot{z})\right] \tag{14}$$

From Eq. (10), the command torque u_4 is as follows;

$$u_4 = K_{p4}(\theta_d - \theta) + K_{d4}(\dot{\theta}_d - \dot{\theta}) \tag{15}$$

In Eqs. (9)~(14), K_p and K_d are the proportional and the derivative gain, respectively. Subscript d means the desired state.

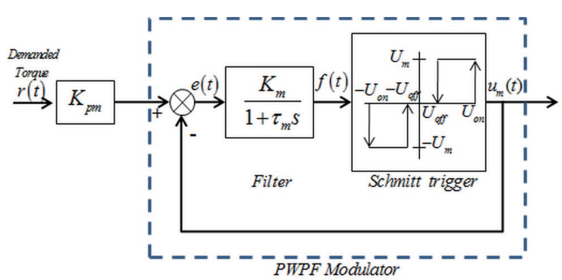

Fig. 3. PWPFM

Table 1. Static Characteristics of PWPFM

On-Time	$t_{on} = -\tau_m \ln\left(1 - \frac{U_{on} - U_{off}}{U_{on} - K_m(R - U_m)}\right)$
Off-Time	$t_{off} = -\tau_m \ln\left(1 - \frac{U_{on} - U_{off}}{K_m R - U_{off}}\right)$
Modulator Frequency	$\frac{1}{t_{on} + t_{off}}$
Duty Cycle	$DC = \frac{t_{on}}{t_{on} + t_{off}}$
Minimum Pulse Width	$\Delta = -\tau_m \ln\left(1 - \frac{U_{on} - U_{off}}{K_m U_m}\right)$

3.2 PWPFM

In the PWPFM, not only the frequency of the pulse but also the distance between the pulses are modulated. Its basic structure is shown in Fig. 3. The modulator includes a Schmitt trigger, a first-order-filter, and a negative feedback loop [5,9,10].

The parameters of interest for designing the PWPFM are as follows: the gain K_m and the time constant τ_m of the first order filter, the Schmitt trigger parameters U_{on}, U_{off}. The static characteristics of the continuous time modulator for a constant input R are presented in Table 1[5,9].

U_m is the output of Schmitt trigger, and U_{on} and U_{off} are the upper and lower boundary value, respectively. In PWPFM, U_{on} and U_{off} are determined by the on-time of pulse[5,9].

3.3 PWM

The basic structure of PWM is shown in Fig. 4. When a positive input to the PWM is greater than a carrier signal,

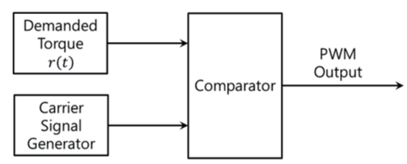

Fig. 4. PWM

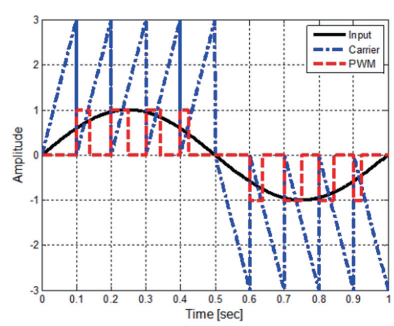

Fig. 5. Time History of PWM

Table 2. Static Characteristics of PWM

On-Time	$t_{on} = \frac{A_{com}}{A_{car}}\frac{1}{f_{car}}$
Off-Time	$t_{off} = \frac{A_{car} - A_{com}}{A_{car}}\frac{1}{f_{car}}$
Modulator Frequency	$MF = \frac{t_{on}}{t_{on} + t_{off}}$
Duty Cycle	$DC = MF \times 100\ (\%)$

the PWM output is ON. If the input falls below a carrier signal, the PWM output is OFF. As shown in Fig. 5, the PWM converts an analog signal into an ON/OFF signal.

The parameters of interest for designing the PWM are as follows: the amplitude of carrier signal A_{car}, the frequency of carrier signal f_{car}. The on-time of the PWM output is determined by A_{car} and f_{car}. The static characteristics of the PWM are presented in Table 2. A_{com} is the control signal from the path tracking controller in Table 2 [11].

4. Simulation

4.1 Mass Properties and Allocation of Thrusters

Mass properties of the demonstrator are set as follows. [12]

$$I_b = \begin{bmatrix} 37.37 & -0.44 & -0.52 \\ -0.44 & 49.22 & 0.35 \\ -0.52 & 0.35 & 48.53 \end{bmatrix} \left(kg \cdot m^2\right)$$

$$m = 100 - 0.7t \left(kg\right)$$

Five main thrusters for altitude control and 8 reaction thrusters for attitude control are applied on the demonstrator, as shown in Fig. 6. A main thruster and a reaction thruster can generate the 200N and 2.96N thrust, respectively. For generating the torque, reaction thrusters can be chosen according to the reaction thruster selection in Table 3.

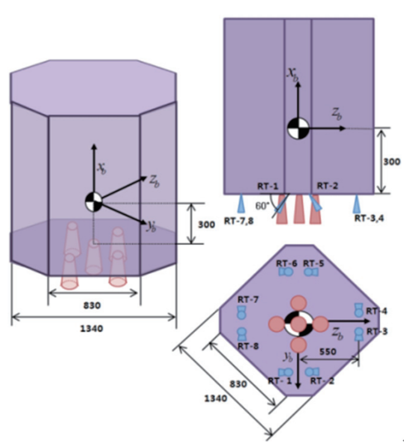

Fig. 6. Configuration of the Demonstrator

Table 3. Reaction Thruster Selection Table

Rotational Motion	Reaction Thruster ID (RT-No.)							
	1	2	3	4	5	6	7	8
$+\phi$	0	0	1	0	0	0	1	0
$-\phi$	0	0	0	1	0	0	0	1
$+\theta$	0	0	1	1	0	0	0	0
$-\theta$	0	0	0	0	0	0	1	1
$+\psi$	0	0	0	0	1	1	0	0
$-\psi$	1	1	0	0	0	0	0	0

4.2 Scenario

The scenario for the simulation consists of 4 phases: ascent, horizontal movement, descent, and touchdown. Fig. 7 represent the desired path of lunar lander demonstrator. The flight time of the simulation is set as 40 seconds [12]. The demonstrator ascends up to 20 m altitude for 15 seconds and moves horizontally by changing the attitude. After that, the demonstrator descends and hovers at the level of 0.3m. When the following three conditions are satisfied simultaneously, all of the thrusters are cut off.

① Altitude: +0.33m ≥ Alt ≥ +0.27m
② Altitude Rate: ≥+0 m/s
③ Simulation Time: >35 sec

4.3 Simulation Result

The designed parameters of PWPFM and PWM are shown in Table 5.

Figures 8-15 are the results of the translation motion, and Figs. 16-23 are the results of the rotational motion. Figs. 24-29 represent force and torque generated from thrusters, respectively. Figs. 30 and 31 represent the three dimensional trajectory of the lunar lander demonstrator. The comparison results of the 3-dimensional position error are shown in Fig. 32. Fis. 33 represents the area of position error with respect to time. As shown in Fig. 33, the error area of PWM based thruster controller is more than those of PWPFM based thruster controller by 21.01m·s. Figs. 34 and 35 represent the total impulse with respect to the thruster. As shown in Figs. 34, PWPFM based main thruster controller use more total impulse than PWM based thruster controller by 155 N·s(3.1%). And

Table 4. Simulation Scenario

Phase		Time(sec)	Target Position(m)
1	Ascent	0~15	(20, 0, 0)
2	Horizontal Movement	15~25	(20, 10, -10)
3	Descent	25~40	(0.3, 10, -10)
4	Touchdown	Engine cut off conditions	(0, 10, -10)

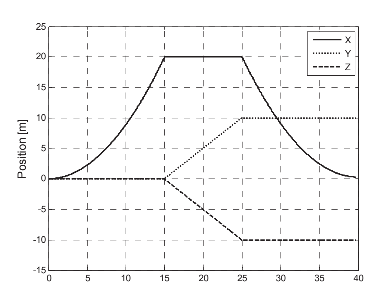

Fig. 7. Desired Path

PWM based reaction thruster controller use more total impulse than PWPFM based thruster controller by 115.25 N·s (77.1%) as shown in Fig. 35. In comparison with the total impulse of both main and reaction thruster, PWPFM based controller use more total impulse than PWM based controller by 39.8 N·s. The final velocity and the final position error are shown in Table 6.

Table 5. Designed Parameters of Modulator

	PWPFM	PWM
Main Thruster	K_{p_m} : 1.4 K_m : 4 τ_m : 0.2 U_{on} : 430 U_{off} : 58.2 U_m : 200	A_{car} : 500 f_{car} : 10
Reaction Thruster	K_{p_m} : 1.4 K_m : 7 τ_m : 0.1 U_{on} : 6 U_{off} : 1.634 U_m : 2.96	A_{car} : 8 f_{car} : 10

Table 6. Comparison Final State of the Lunar Lander Demonstrator

Thuster Control Type	PWPFM	PWM
Landing Time (s)	39.685	40
Final Velocity (m/s)	X : -2.7068 Y : 0.1065 Z : -0.0190	X : 0.3810 Y : 0.0643 Z : -0.1137
Final Position Error (m)	X : -0.3090 Y : 1.2929 Z : -0.9781	X : 0.0487 Y : -0.8527 Z : 0.5631

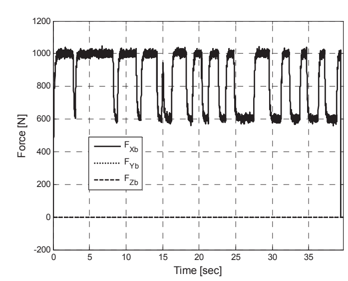

Fig. 8. Total External Force (PWPFM)

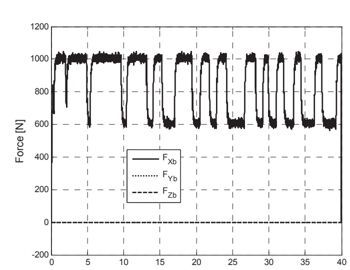

Fig. 9. Total External Force (PWM)

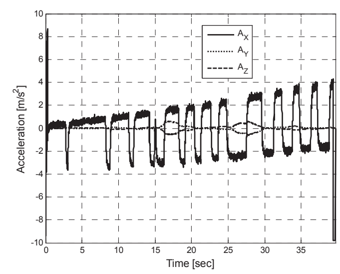

Fig. 10. Inertial Acceleration (PWPFM)

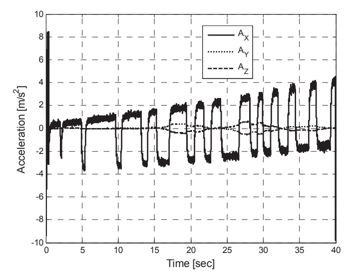

Fig. 11. Inertial Acceleration (PWM)

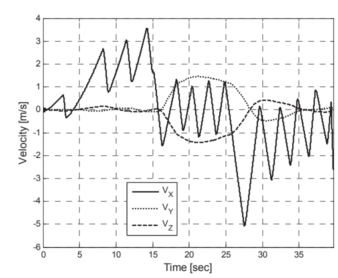

Fig. 12. Inertial Velocity (PWPFM)

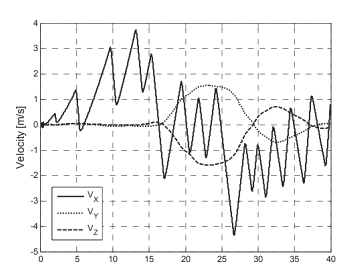

Fig. 13. Inertial Velocity (PWM)

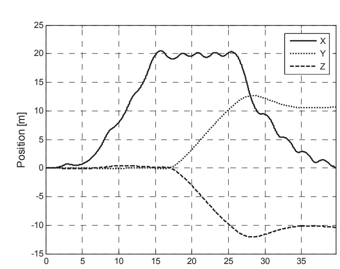

Fig. 14. Inertial Position (PWPFM)

DOI: http://dx.doi.org/10.5139/IJASS.2015.16.1.102

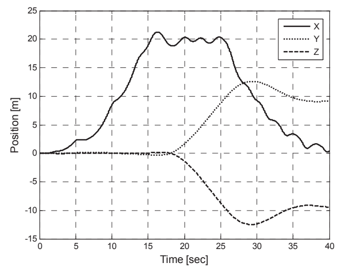

Fig. 15. Inertial Position (PWM)

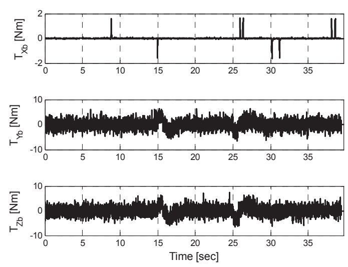

Fig. 16. Total External Torque (PWPFM)

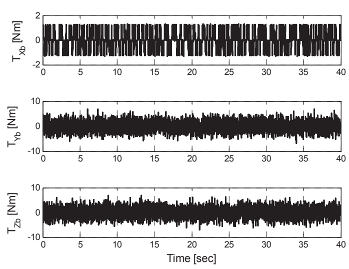

Fig. 17. Total External Torque (PWM)

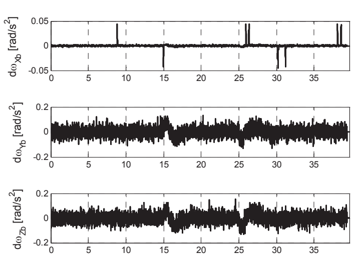

Fig. 18. Angular Acceleration (PWPFM)

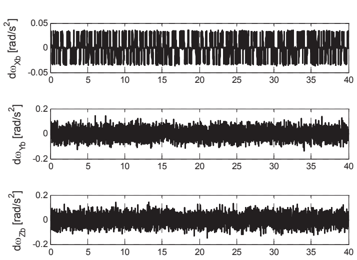

Fig. 19. Angular Acceleration (PWM)

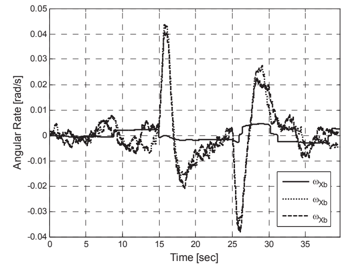

Fig. 20. Angular Rate (PWPFM)

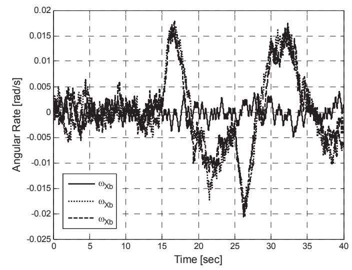

Fig. 21. Angular Rate (PWM)

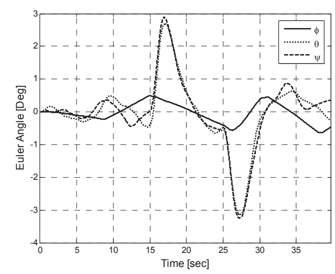

Fig. 22. Euler Angle (PWPFM)

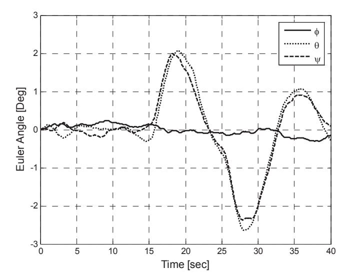

Fig. 23. Euler Angle (PWM)

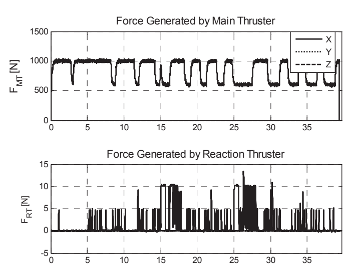

Fig. 24. Force Generated by Main Thruster and Reaction Thruster (PWPFM)

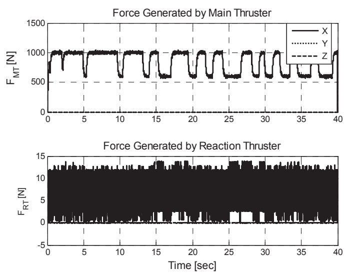

Fig. 25. Force Generated by MT and RT (PWM)

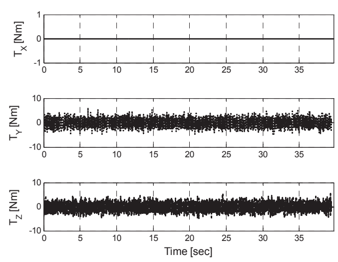

Fig. 26. Torque Generated by MT (PWPFM)

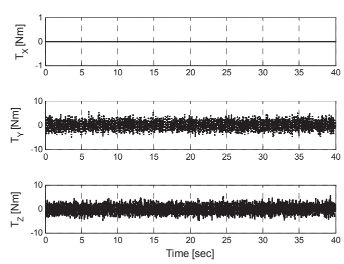

Fig. 27. Torque Generated by MT (PWM)

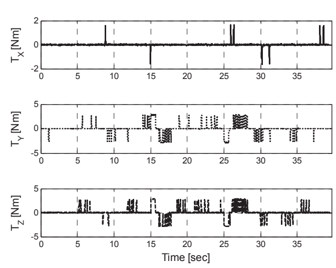

Fig. 28. Torque Generated by RT (PWPFM)

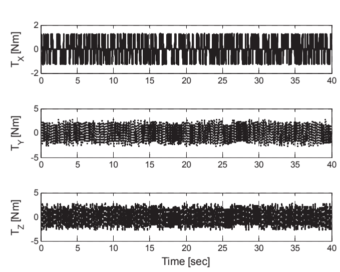

Fig. 29. Torque Generated by RT (PWM)

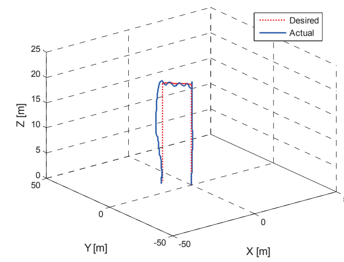

Fig. 30. 3D Trajectory of the Demonstrator (PWPFM)

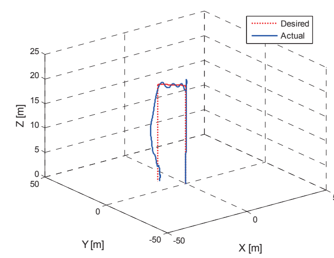

Fig. 31. 3D Trajectory of the Demonstrator (PWM)

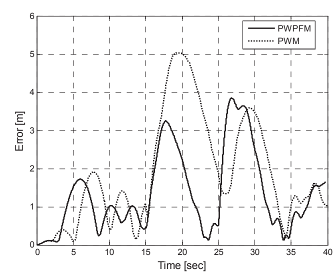

Fig. 32. 3-Dimensional Position Error

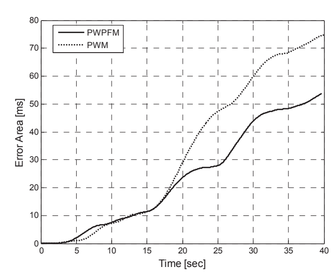

Fig. 33. Area of Position Error

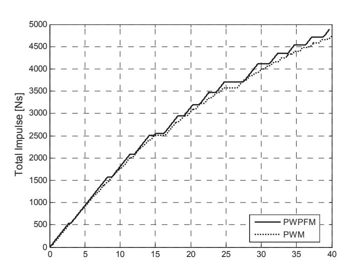

Fig. 34. Total Impulse of Main Thruster

DOI: http://dx.doi.org/10.5139/IJASS.2015.16.1.102

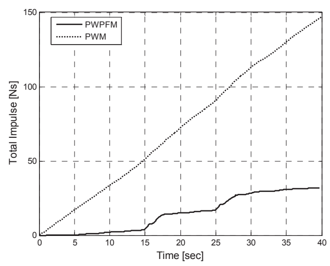

Fig. 35. Total Impulse of Reaction Thruster

5. Conclusion

In this paper, a path tracking controller based on thrusters for the lunar lander demonstrator was designed. For this, we first derived equations of motion by considering the allocation of thrusters. With the equations of motion, we designed the path tracking controller based on Euler angle. The signal generated from the controllers is continuous, so PWPFM and PWM are applied for generating ON/OFF signal. We constructed a 4-phase scenario including ascent, horizontal movement, descent, and touchdown. MATLAB simulations were performed for evaluating the path tracking ability and final landing velocity. The result shows that the proposed controllers of the lunar lander demonstrator can track the desired path well and land on the ground softly. Also, the result shows that PWPFM based thruster controller is slightly better than PWM based thruster controller, from the perspective of path tracking performance, while PWM based thruster controller use less total impulse than PWPFM based controller.

References

[1] D. Rew, K. Ju, S. Lee, K. Kim, S. Kang, and S. Lee, "Control System Design of the Korean Lunar Lander Demonstrator", *Acta Astronautica*, Vol. 94, No. 1, 2014, pp. 328-337.

[2] D. Rew, K. Ju, S. Kang, H. Seo, and S. Lee, "Control System Configuration Design and Dynamics Simulation for Lunar Lander Demonstrator", *KSAS 2011 Conference*, Korea, Sep. 9-11, 2011

[3] B. J. Morse, B. W. Ballard, and C L. B. Reed, "NASA's Robotic Lunar Lander Project Update", *AIAA SPACE 2010 Conference and Exposition*, Anaheim, California, Aug. 30 - Sep. 2, 2010.

[4] R. Frampton, K Oittinen, J. M. Ball, A. Khodadoust, D. Kirshman, G. Grayson, and P. Sundaram, "Planetary Lander Dynamic Model for GN&C", *AIAA SPACE 2009 Conference and Exposition*, Pasadena, California, Sep. 14-17, 2009.

[5] M. J. SIDI, S*pacecraft Dynamics and Control*, Cambridge University Press, New York, 1997, pp. 260-290.

[6] K. L. Zhang, S. K. Chou and Simon S. Ang, "Performance Prediction of a Novel Solid-Propellant Microthruster", *Journal of Propulsion and Power*, Vol. 22, No. 1, 2006, pp.56-63.

[7] Raymond Kristiansen, and David Hagen, "Modeling of Actuator Dynamics for Spacecraft Attitude Control", *Journal of Guidance, Control, and Dynamics*, Vol. 32, No. 3, pp. 1022-1025.

[8] Altuğ E., Ostrowski J. P. and Taylor C. J., "Control of a Quadrotor Helicopter Using Dual Camera Visual Feedback", *The International Journal of Robotics Research*, Vol. 24, No. 5, 2005, pp. 329-341.

[9] T. D. Krovel, *Optimal Tunning of PWPF Modulator for Attitude Control*, Master Thesis, Department of Engineering Cybernetics, Norwegian University of Science and Technology, 2005.

[10] T. C. Anthony and B. Wie, *Pulse Modulated Control Synthesis for a Flexible Spacecraft*, AIAA, 1989, pp. 65-76.

[11] N. Ma and G. Song, "Control of Shape Memory Alloy Actuator using Pulse Width Modulation", *Smart Materials and Structure*, Vol. 12, No. 5, 2003, pp. 712-719.

[12] K. Kim, J. Lee, S. Lee, S. Ko, D. Rew and G. Ju, "Path Tracking Controller Design and Simulation for the Lunar Lander Demonstrator", *AIAA Modeling and Simulation Technologies Conference*, Minneapolis, Minnesota, Aug. 13-16, 2012.